Journal of Chromatography A, 1218 (2011) 5010–5019

Contents lists available at ScienceDirect

Journal of Chromatography A

journal homepage: www.elsevier.com/locate/chroma

Effect of monomer mixture composition on structure and chromatographic properties of poly(divinylbenzene-*co*-ethylvinylbenzene-*co*-2-hydroxyethyl methacrylate) monolithic rod columns for separation of small molecules

Konstantin N. Smirnov*, Ivan A. Dyatchkov, Maxim V. Telnov, Andrey V. Pirogov, Oleg A. Shpigun

Analytical Chemistry Division, Chemistry Department, Lomonosov Moscow State University, Lenin Hills, 119991 Moscow, Russia

ARTICLE INFO

Article history:
Available online 13 December 2010

Keywords:
Porous polymer monolith
Divinylbenzene
2-Hydroxyethyl methacrylate
Nitrogen adsorption
HPLC
Small molecules

ABSTRACT

Porous poly(divinylbenzene-*co*-ethylvinylbenzene-*co*-2-hydroxyethyl methacrylate) monoliths were synthesized via thermally initiated free-radical polymerization in confines of surface-vinylized glass columns (150 mm × 3 mm i.d.) and applied to the reversed-phase separation of low-molecular-weight aromatic compounds. In order to compensate for the polymer shrinkage during the synthesis and prevent the monolith from detachment from the column wall, polymerization was conducted under nitrogen pressure. The reaction proceeded at 60 °C for 22 h. 2,2′-Azo-*bis*-isobutironitrile was used as the initiator and 1-dodecanol was used as the porogen. A series of monoliths with different monomer ratios were obtained. All the monoliths had high specific surface areas ranging from 370 to 490 m^2/g. In the studied range of monomer mixture compositions, the mechanical stability of the stationary phase in water/acetonitrile eluents was found to be high enough and practically insensitive to the fraction of 2-hydroxyethyl methacrylate (HEMA). Increasing the molar fraction of HEMA from 10.5% to 14.7% resulted in the decrease of column permeability by two orders of magnitude (from 1.1×10^{-12} to 1.8×10^{-14} m^2) and led to weaker retention of alkylbenzenes. The higher HEMA content was shown to reduce the plate height of the columns in the separation of small molecules from 160–490 μm to 40–76 μm. This was attributed mainly to the decrease of the domain size of the monoliths leading to lower eddy dispersion and mass transfer resistance in the column.

1. Introduction

In recent years, monolithic stationary phases for liquid chromatography have attracted considerable attention because of their unique structure, which can be tailored at the stage of the monolith synthesis [1]. Several review articles [2–8] devoted to the methods of preparation, properties, and various applications of monolithic columns have been published. Porous polymer monoliths are widely used as the stationary phases for the separation of biomacromolecules in gradient elution mode [5–7]. The rapid, high-resolution separations of proteins, peptides, and nucleic acids are provided by the combination of the fast mass transfer kinetics with high hydrodynamic permeability of the monoliths and strong dependency of retention of multifunctional macromolecules on the mobile phase composition. However, performance of polymeric monoliths in the isocratic separation of low-molecular-weight organic compounds with similar properties is relatively poor. Different possible reasons for this are discussed in paper [9]. Development of the polymer-based monolithic columns for the HPLC of small organic molecules is an important problem. Emerging studies that address this problem mostly deal with the preparation of monoliths inside fused-silica capillaries [9–14]. This is caused largely by the simplicity of the monolith covalent bonding to the modified inner wall of a narrow-bore capillary having large surface-to-volume ratio. However, the application of capillary monoliths requires the equipment affording very low flow rates, small injection volumes, and minimal extra-column and detector cell volumes while many analytical laboratories are still equipped only with conventional chromatographs, which are unable to operate with micro-bore columns. Therefore, development of the monolithic columns with conventional analytical dimensions (2–5 mm i.d.) for the separation of small molecules is desirable.

Unfortunately, because of the polymer shrinkage accompanying the polymerization process and the difference in reaction kinetics, which arises from the difference in the rate of heat transfer inside various molds, it is more difficult to prepare efficient, radially homogeneous, and strongly adhered to the column inner wall polymeric monolith inside a tube with a diameter of several millimeters than inside a capillary [3,15,16]. Svec and Fréchet [17]

* Corresponding author. Tel.: +7 495 939 46 08; fax: +7 495 939 32 41.
E-mail address: smirnov-const@yandex.ru (K.N. Smirnov).

0021-9673/$ – see front matter © 2010 Elsevier B.V. All rights reserved.
doi:10.1016/j.chroma.2010.12.025

stated that conducting the polymerization slowly inside an upright standing tube was sufficient to avoid channeling at the column wall–monolith interface since the free space created by radial shrinkage of the polymer was filled with the liquid polymerization mixture remaining at the top of growing monolith. Allington et al. [18] suggested conducting the synthesis of conventional-diameter monoliths under pressure to prevent the formation of the voids between the monolith and the column wall. The pressure can be applied to the column with a piston or a gas filling the space above the polymerization mixture. The column wall may be either untreated or modified before the synthesis in order to improve adhesion of the polymer to the wall. The authors [18] claim that the monoliths prepared under pressure are more reproducible and efficient than those prepared inside hermetically sealed tubes. Soft monoliths can also be compressed after the synthesis as proposed in the pioneering work by Hjertén et al. [19], but this approach requires special columns with movable end-fittings. Another possible way to provide a leakproof contact of the polymeric rod with the column wall is to use the cladding process of the pre-formed and dried monolith [20] similar to the process used in the fabrication of conventional-diameter silica monolithic columns [2,3]. However, this approach is more difficult to implement for non-rigid polymers than for silica, and it is more laborious than the *in situ* polymer synthesis. To reduce the monolith radial heterogeneity caused by the gradient of temperature across the mold, controlled heating of the reaction mixture and radiation induced polymerization were suggested [8,21].

An important issue that also should be taken into account in the synthesis of conventional-bore polymeric monoliths is that even a properly prepared monolith can detach from the wall later if the column is operated with the mobile phase in which the polymer shrinks. In the case of hydrophobic monoliths used for the reversed-phase chromatography, a mixture containing low percentage of organic modifier in water may cause such an effect. To avoid this problem, the stationary phase hydrophobicity can be adjusted by changing the composition of the monomer mixture used for the monolith synthesis, or post-polymerization modification of the monolith [18].

In 1998, Xie et al. [22] obtained a monolith based on a copolymer of divinylbenzene (DVB), ethylvinylbenzene (EVB), and a hydrophilic monomer 2-hydroxyethyl methacrylate (HEMA) inside a 1 mm i.d. poly(ether ether ketone) tube and applied it to the solid-phase extraction of phenols from water samples. The improved wettability of the monolith and higher recoveries of polar compounds in comparison with poly(DVB-*co*-EVB) adsorbent were reported. However, little information about the influence of the amount of HEMA in the polymerization mixture on the monolith properties was provided. The purpose of the present study was to prepare monolithic columns based on poly(DVB-*co*-EVB-*co*-HEMA) with conventional analytical dimensions (150 mm × 3 mm i.d.) for the reversed-phase separation of small molecules. Here, for the first time, we report on a detailed investigation of the effect of the monomer mixture composition on the porous characteristics, mechanical stability, and chromatographic properties of these columns.

2. Experimental

2.1. Chemicals and materials

DVB (a mixture containing 80% of 1,3-DVB + 1,4-DVB and 20% of 1-ethyl-3-vinylbenzene + 1-ethyl-4-vinylbenzene), HEMA (97%), 2,2′-azo-*bis*-isobutironitrile (AIBN, >98%), 3-(trimethoxysilyl)propyl methacrylate (98%), 1-dodecanol (>98%), uracil (≥99%), nitrobenzene (>99%), ethylbenzene (≥99%), propylbenzene (98%) were purchased from Sigma–Aldrich (St. Louis, MO, USA). Toluene (>98%) was from Reakhim (Moscow, Russia). HPLC-gradient grade acetonitrile was from Panreac (Barcelona, Spain). Water was purified with a Milli-Q system (Millipore, Bedford, MA, USA). All the other solvents and chemicals were of reagent or analytical grade. For chromatographic studies, sample solutions with concentrations of 40–50 μg/ml of uracil or thiourea, 500 μg/ml of nitrobenzene, and 1000 μg/ml of pyridine and alkylbenzenes were prepared in the mobile phases used.

Monoliths were synthesized inside glass tubes with nominal length of 150 mm and i.d. of 3 mm. The tubes and steel column holders with special end-fittings were purchased from Tessek (Prague, Czech Republic). The accurate volumes of the empty tubes were determined via pycnometry, weighing the amount of a solvent (chloroform) needed to fill the column and dividing the solvent mass by its density. The obtained column lengths and internal diameters were in the ranges of 147–148 mm and 3.23–3.32 mm, respectively.

2.2. Column fabrication

To provide covalent attachment of the monolith to the column wall, the surface of glass tube was vinylized according to the procedure described in Ref. [23] with minor modifications. To activate the surface, the tube was filled with 1 M aqueous sodium hydroxide, sealed with polypropylene caps, placed into a 1 l beaker filled with just-boiled water, and left for 1 h. Then the column was flushed with water, and the same procedure was repeated using 1.2 M HCl instead of NaOH. Next, the column was rinsed sequentially with water and acetone, filled with a 30 wt% solution of 3-(trimethoxysilyl)propyl methacrylate in acetone, and left for 22 h at room temperature. After vinylization, the tube was rinsed with acetone and dried in air.

Polymerization mixture containing 38 wt% of monomers, 62 wt% of 1-dodecanol as the porogen, and 1 wt% (with respect to monomers) of AIBN as the initiator was prepared in a glass vial and purged with nitrogen for 10 min. The relative amounts of HEMA and DVB were varied (Table 1). Since HEMA and DVB have equal molar weights, the molar fraction of AIBN with respect to monomers remained constant (0.8%) for all the mixtures.

In order to compensate for the polymer shrinkage during the synthesis and prevent the monolith from detachment from the column wall, polymerization was conducted under pressure of nitrogen as proposed in Ref. [18]. Since the volume of reacting mixture decreased during the polymerization, a glass pre-column (30 mm × 3 mm i.d., Tessek) was connected to the upper end of the surface-vinylized main column while the lower end of the main column was closed with a polypropylene cap. When placed inside the steel column holder, the column and pre-column were pushed against each other, compressing a PTFE ring placed between them and providing a leakproof connection withstanding pressures up

Table 1
Recipes of the monoliths considered in this study.

Monolith	Polymerization mixture (wt%)[a]		
	HEMA	DVB[b]	1-Dodecanol
M-40	4.0 (10.5)	34.1 (89.5)	61.9
M-45	4.5 (11.9)	33.4 (88.1)	62.1
M-50	5.0 (13.2)	33.1 (86.8)	61.9
M-56	5.6 (14.7)	32.5 (85.3)	61.9
M-68	6.8 (17.9)	31.3 (82.1)	61.9
M-80	8.0 (21.1)	30.0 (78.9)	62.0

[a] AIBN was used as the initiator (1 wt% with respect to monomers). Given in parentheses are the molar percentages with respect to the total amount of monomers.
[b] A mixture containing 80% of 1,3-DVB + 1,4-DVB and 20% of 1,3-EVB + 1,4-EVB.

to 6 bar. This setup was filled with the polymerization mixture and connected to a reservoir with nitrogen. The gas pressure was set at 3 bar (excess over the atmospheric pressure), and the setup was immersed in a vertical position into a water thermostat preheated to 60 °C. The reaction proceeded for 22 h. In this study, the polymerization pressure was not optimized. After the reaction, the setup was cooled for 20 min to about 30–40 °C, the pressure applied was gradually decreased, and the column was taken out of the steel holder. The pre-column was disconnected, and the excess of polymer was carefully removed from the ends of the column to obtain flat surfaces. The column was supplied with end-fittings and placed inside the steel column holder. Then acetonitrile (25 ml) was pumped through the monolith to remove the porogen and unreacted monomers. The wash volume was collected for the monomer conversion studies.

2.3. Instrumentation and analytical methods

Monomer conversion was determined with an Agilent 6850A gas chromatograph (Waldbronn, Germany) coupled to an Agilent 5973N quadrupole mass spectrometric detector. A Zebron ZB-WAX (60 m × 0.25 mm i.d., 0.25 μm film thickness) capillary column (Phenomenex, Torrance, CA, USA) was used for the analysis. The carrier gas was helium, and the analysis was performed at a flow rate of 1 ml/min. A volume of 1 μl of appropriately diluted initial polymerization mixture or solution obtained after the post-synthesis wash of the monolith was injected. The split ratio was set at 5:1. The injector and the detector transfer line temperatures were 240 °C. The GC oven temperature was programmed from 50 °C (held for 3 min) to 230 °C at 10 °C/min, and then held at 230 °C for 4 min. For quantification, chromatograms were acquired in selected ion monitoring mode. The monomer conversion, q, was calculated according to the following equation:

$$q(\%) = 100 \times \left(1 - \left(\frac{S_{\text{monomer},2}}{S_{\text{dodecanol},2}}\right) / \left(\frac{S_{\text{monomer},1}}{S_{\text{dodecanol},1}}\right)\right) \quad (1)$$

where $S_{\text{monomer},1}$ and $S_{\text{dodecanol},1}$ are the peak areas of the monomer and the porogen, respectively, in the initial polymerization mixture, and $S_{\text{monomer},2}$ and $S_{\text{dodecanol},2}$ are the corresponding peak areas in the solution obtained after the post-synthesis wash step.

Chromatographic evaluation of the fabricated columns was performed on an Agilent 1200 Series liquid chromatograph (Waldbronn, Germany) equipped with a quaternary pump, a vacuum degasser, an autosampler, a column thermostat, a diode array UV detector, and a data station. All the chromatographic experiments were conducted at a constant temperature of 25 °C maintained by the column thermostat. The injection volume was 1 μl. The UV detection was carried out at 210 nm. The data acquisition rate was 20 Hz. All the retention data points reported hereafter are the mean values of three consecutive injections. They were corrected for the extra-column volume (57 μl) measured from the autosampler needle seat to the detector flow cell. Corrected for the extra-column contribution heights equivalent to a theoretical plate (HETP) were calculated according to the following equation [24]:

$$H = L\frac{w_{1/2}^2 - w_{1/2,e}^2}{5.545(t_R - t_e)} \quad (2)$$

where H is the HETP, L is the column length, t_R is the gross retention time of the compound, t_e is the retention time of the same compound measured using the same mobile phase at the same flow rate with a zero-volume union installed instead of the column, and $w_{1/2}$ and $w_{1/2,e}$ are the corresponding peak-widths at half height.

The HETP versus the mobile phase velocity curves were obtained by running analyses of a solution containing uracil and toluene from the lower velocity to the higher one, then back to the lower, and again to the higher. The average values of these three HETP measurements are reported elsewhere in this article. The relative standard deviations of HETP do not exceed 5.3% for uracil and 2% for toluene, indicating the stability of the columns over the studied velocity and pressure ranges. The HETP curves were fitted with Knox's equation [25]:

$$H = Au^n + \frac{B}{u} + Cu \quad (3)$$

where u is the chromatographic linear velocity; A, B, C, and n were considered as four independently variable parameters. The fitting was carried out with the solver function of Microsoft Excel 2003.

For hydrodynamic permeability determination, the monolithic column was connected to the chromatograph, and the pressure drop at various flow rates was recorded. After subtracting the system pressure drop, the one generated by the column was obtained. The permeability was calculated from the slope of the plot of the column pressure drop against the flow rate.

After chromatographic experiments, the monolith total porosity was determined via pycnometry. The column was flushed with acetonitrile and weighed. Then the column was dried at ambient temperature for several days and then dried in vacuum at 40 °C until the constant weight was reached. The weight of acetonitrile was divided by the solvent density to obtain the total pore volume. By dividing the total pore volume by the empty tube volume, the total porosity was obtained. The relative uncertainty in the value of porosity does not exceed 1%.

A Supra 50VP scanning electron microscope (Carl Zeiss, Oberkochen, Germany) was used for observing the monolith morphology in the dry state. The images were acquired with a VPSE-detector in a low vacuum mode at an accelerating voltage of 20 kV. Nitrogen adsorption–desorption isotherms at 77 K were obtained with a Micromeritics ASAP 2000 analyzer (Norcross, GA, USA). After pycnometry, the monolith was extruded from the glass tube and cut into pieces. A 0.1–0.2 g sample was outgassed at 150 °C to the residual pressure of 0.005 mm Hg prior to data collection. The specific surface area was determined according to the Brunauer–Emmett–Teller (BET) method [26] using eight-point adsorption isotherm between 0.05 and 0.20 relative pressure of N_2. Pore size distribution was obtained by the Barrett–Joyner–Halenda (BJH) analysis [27] of the adsorption branch of the isotherm with the assumption of cylindrical pore geometry and the statistical thickness of the adsorbed film calculated using the Harkins–Jura equation [28].

3. Results and discussion

3.1. Monomer conversion

The monomer conversions determined by GC/MS analysis are presented in Fig. 1. Since the monolith synthesis was conducted under constant pressure of nitrogen that served as a compensation for the polymer shrinkage, the exact volume of the mixture polymerized in confines of the glass tube was unknown. Therefore, the monomer conversions were calculated by comparison of the monomer-to-porogen ratios in the initial polymerization mixture with those in the wash solution (Eq. (1)). The GC peaks of all the monomers and 1-dodecanol were base-line separated; divinylbenzenes were distinguished from ethylvinylbenzenes by their mass spectra, but it was more difficult to identify the isomers. Despite the lack of the standards of the individual isomers, the DVB isomer with higher conversion was identified as 1,4-DVB and that with lower one as 1,3-DVB since it was known [29] that 1,4-DVB is slightly more reactive than 1,3-DVB in free-radical polymerization. Ethylvinylbenzenes have similar conversions (difference within 1%), and the average values for these monomers are shown

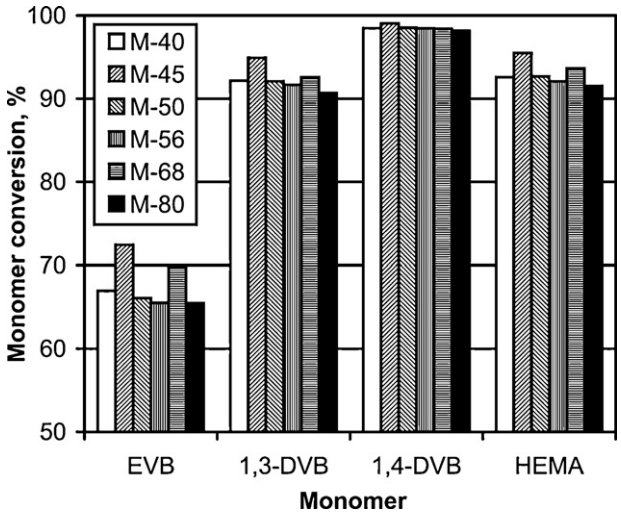

Fig. 1. Monomer specific conversion determined by GC/MS for the monoliths synthesized inside 150 mm × 3 mm i.d. surface-vinylized glass tubes under nitrogen pressure (4 bar) at 60 °C for 22 h. For the monolith recipes, see Table 1.

in Fig. 1. It is evident that the monomer conversions are rather high and practically independent of the composition of the initial polymerization mixture. Although some oligomeric products could be formed during the syntheses and could not be quantified by GC/MS analysis, one can conclude overall that the monomer ratio in the final monolith is proportional to that in the initial monomer mixture. Thus, the increase of the HEMA content in the polymerization mixture results in the monolith with proportionally higher amount of hydrophilic monomer and with lower cross-link density.

3.2. Monolith morphology

Scanning electron micrographs (SEM) of the obtained poly(DVB-*co*-EVB-*co*-HEMA) monoliths are shown in Fig. 2. The images reveal microglobular morphologies typical for polymeric monoliths. The increase of the weight fraction of HEMA in the polymerization mixture from 4% to 8% leads to a dramatic drop in the size of globules comprising the polymers and, consequently, the size of the interstices between these globules. This fact can be explained in terms of the improvement of the polymer–porogen interactions [30]. 1-Dodecanol is a thermodynamically poor solvent for styrenic polymers. However, the presence of a hydroxyl group in its molecule makes it a good solvating agent for HEMA. The increase of the amount of HEMA in the polymerization mixture results in polymers with higher numbers of hydroxyl groups; hence, these polymers are more strongly solvated by 1-dodecanol. This delays the onset of phase separation during the polymerization and lowers the local concentration of monomers within the swollen phase-separated nuclei, leading to slower growth of the polymeric microglobules. In addition, newly formed nuclei obtained in the solution have weaker tendencies to be adsorbed by the globules formed earlier and retain more individuality. On the other hand, the increase of the amount of HEMA is accompanied by the decrease of the cross-linker amount (molar fraction of DVB decreases from 72% to 63% with respect to the total amount of monomers) that usually results in the formation of monoliths consisting of larger globules [30]. Obviously, in the present case, the effect of the porogen solvating strength dominates over the effect of cross-link density.

In our preliminary experiments, we used polymerization mixtures which included 54 wt% of 1-dodecanol and 8 wt% of toluene, the latter being a good solvent for styrenic polymers. In that case, the complicated pattern of polymer–solvent interactions did not allow preparing the monoliths with reasonably large macropores from the mixtures containing more than 3 wt% of HEMA. Therefore, for further studies, 1-dodecanol was chosen as the sole porogen.

3.3. Nitrogen adsorption

Porous properties of the monoliths in the dry state were investigated by low-temperature nitrogen adsorption method. The nitrogen adsorption–desorption isotherms on the monoliths are shown in Fig. 3. According to the IUPAC recommendations [31], the isotherm of the monolith M-40 can be classified as a combination of types I and IV, which is characteristic of solids containing both micropores (<2 nm) and mesopores (2–50 nm). The type H2 hysteresis loop of this isotherm can be attributed to the presence of ink-bottle pores or pore network effects [32]. Micropores and bad pore connectivity are undesirable features of the structure of a chromatographic adsorbent since they hinder the mass transfer of

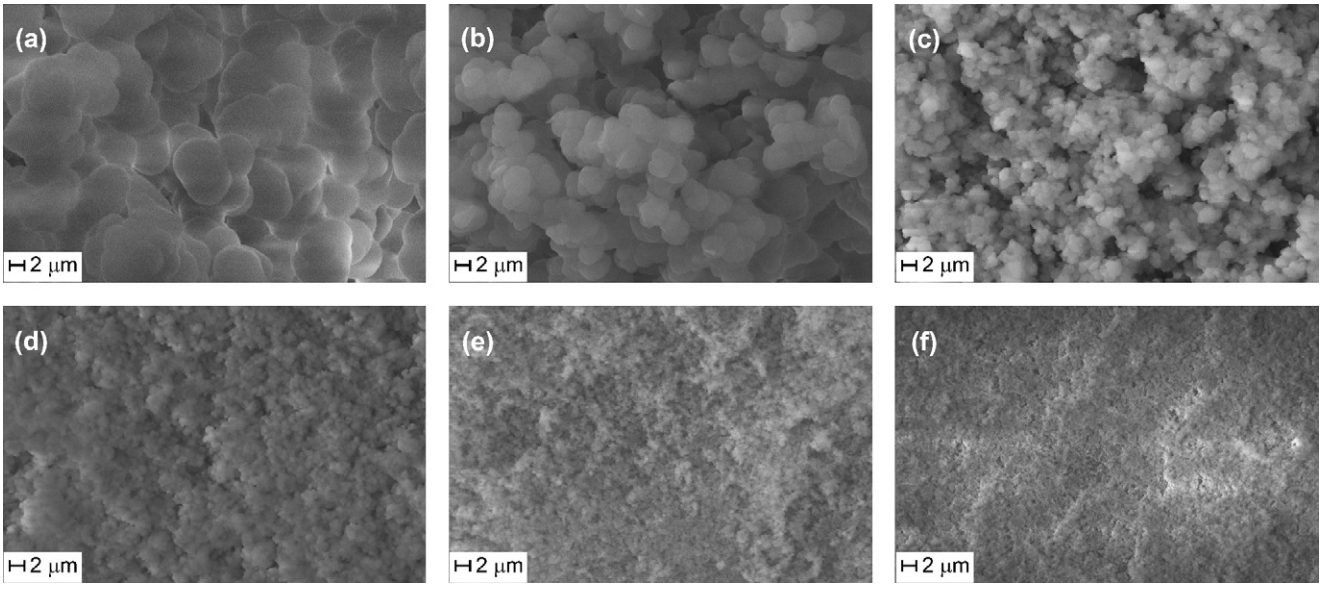

Fig. 2. SEM images of the synthesized poly(DVB-*co*-EVB-*co*-HEMA) monoliths: (a) M-40, (b) M-45, (c) M-50, (d) M-56, (e) M-68, and (f) M-80. For the monolith designations, see Table 1.

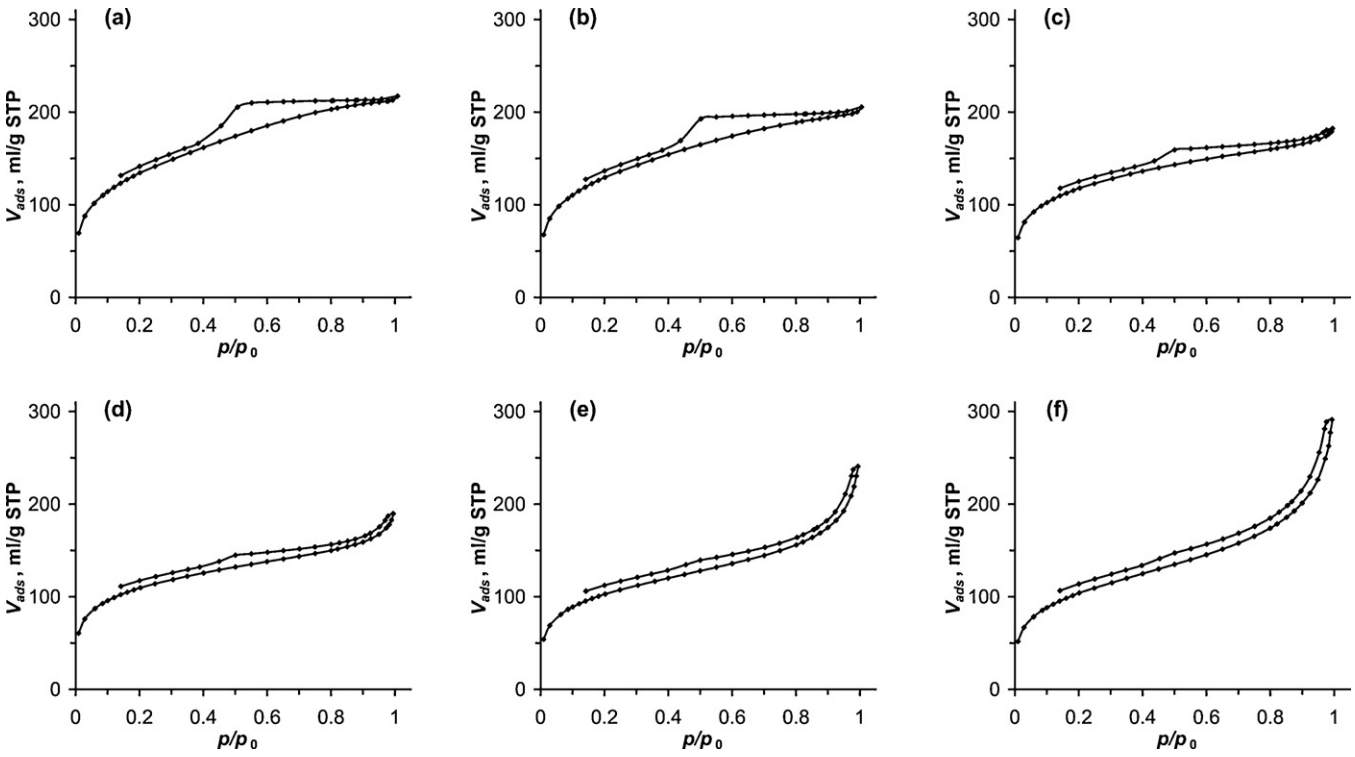

Fig. 3. Nitrogen adsorption–desorption isotherms at 77 K on the synthesized poly(DVB-*co*-EVB-*co*-HEMA) monoliths: (a) M-40, (b) M-45, (c) M-50, (d) M-56, (e) M-68, and (f) M-80. For the monolith designations, see Table 1.

the analytes during the separation [33]. The increase of the weight fraction of HEMA in the polymerization mixture from 4% to 5.6% gradually changes the shapes of the isotherms into a more pronounced type I with smaller hysteresis loop. Further increase of the HEMA amount leads to the isotherms of type IV with long hysteresis loops indicating broad distributions of pore sizes. The low pressure hysteresis (at $p/p_0 < 0.42$) seen in all the isotherms may be associated with the irreversible entrapment of nitrogen in pores of about the same width as that of the adsorbate molecule [31].

The main characteristics of the synthesized monoliths derived from the isotherms are presented in Table 2. All the monoliths have high BET surface areas decreasing from M-40 to M-80. The value of surface area is mainly determined by the amount of micropores and small mesopores (2–10 nm). Usually, the specific surface area of a polymer grows with the increase of the porogen solvating strength and the increase of the amount of cross-linker [34]. As discussed in Section 3.2, the solvation of poly(DVB-*co*-EVB-*co*-HEMA) by 1-dodecanol improves from M-40 to M-80 while the amount of cross-linker decreases in the same order. On the one hand, the volume of small mesopores falls from M-40 to M-56 as determined by the BJH method (Fig. 4). The mesopores in these monoliths are formed mainly by the interstices between the finest primary particles that comprise the microglobules seen in Fig. 2a–d. As the size of microglobules decreases from M-40 to M-56, the total volume of mesopores inside these microglobules decreases as well. From M-56 to M-80, the volume of mesopores rises again since the microglobules become so small that a large fraction of mesopores in this case is formed by the voids between the microglobules themselves. On the other hand, the sharpening of the isotherm knee at low p/p_0 evidenced by the increase of the BET C values from M-40 to M-56 (Table 2) suggests the increase of the volume of micropores in the same order although higher C values can also result from the enhanced interaction of nitrogen molecules with the polymer. The specific volume of micropores obtained using the t-plot method [32] with the Harkins–Jura t-curve increases indeed from 0.017 ml/g for M-40 to 0.040 ml/g for M-56 and falls to 0.013 ml/g for M-80 (Table 2). However, the linearity of the obtained t-plots in the range of film thicknesses of 3.5–5 Å is mod-

Table 2
Characteristics of the obtained poly(DVB-*co*-EVB-*co*-HEMA) monoliths in the dry state determined from nitrogen adsorption isotherms at 77 K.

Monolith	S_{BET} (m^2/g)[a]	C[b]	V_{pore} (ml/g)[c]	V_{BJH} (ml/g)[d]	$V_{micropore\ BJH}$ (ml/g)[e]	$V_{micropore}$ (ml/g)[f]
M-40	490	97	0.330	0.212	0.118	0.017
M-45	470	105	0.310	0.190	0.119	0.021
M-50	420	161	0.282	0.159	0.123	0.037
M-56	390	195	0.294	0.178	0.115	0.040
M-68	370	140	0.372	0.275	0.097	0.029
M-80	380	94	0.450	0.367	0.083	0.013

For the monolith designations, see Table 1.
[a] Specific surface area calculated according to the BET method.
[b] BET C value.
[c] Specific volume of pores with diameters less than 300 nm calculated from the volume of nitrogen adsorbed at p/p_0 0.995.
[d] Cumulative specific volume of pores with diameters between 2 and 300 nm calculated by the BJH method.
[e] Specific volume of micropores (<2 nm) calculated as a difference between V_{pore} and V_{BJH}.
[f] Specific volume of micropores obtained with the t-plot method.

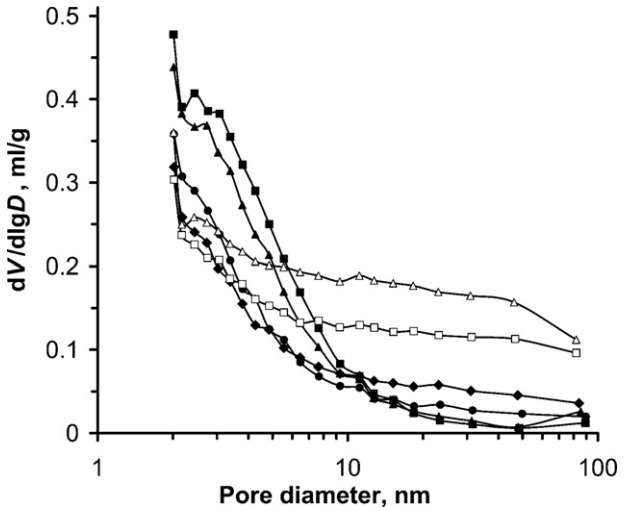

Fig. 4. Differential pore size distributions of the synthesized poly(DVB-*co*-EVB-*co*-HEMA) monoliths derived from the BJH analysis of the nitrogen adsorption isotherms: (■) M-40, (▲) M-45, (●) M-50, (♦) M-56, (□) M-68, and (△) M-80. For the monolith designations, see Table 1.

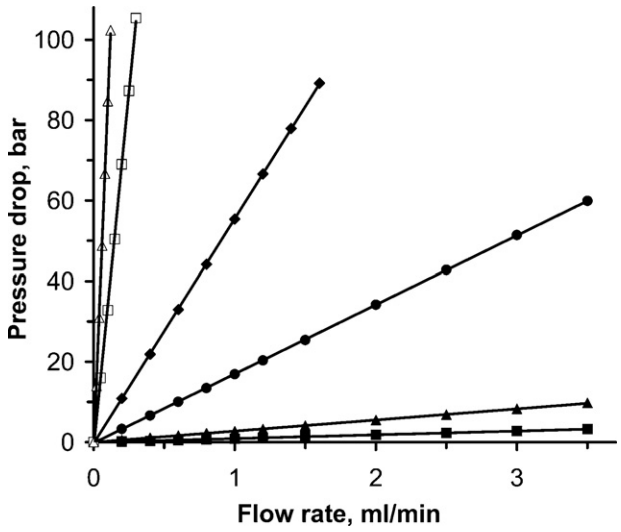

Fig. 5. Plot of the column pressure drop versus the mobile phase flow rate for the obtained 150 mm × 3 mm i.d. poly(DVB-*co*-EVB-*co*-HEMA) monolithic columns: (■) M-40, (▲) M-45, (●) M-50, (♦) M-56, (□) M-68, and (△) M-80. Mobile phase: acetonitrile. Column temperature: 25 °C. For the monolith designations, see Table 1.

erate (R^2 = 0.9912–0.9952); thus, the accuracy of the *t*-plot method is rather questionable in the present case. The micropore volume was also estimated as a difference between the total volume of pores with diameters less than 300 nm, calculated from the volume of nitrogen adsorbed at p/p_0 0.995, and the BJH cumulative pore volume. The BJH method is known to underestimate pore sizes [32], and the micropore volume calculated in such a way is likely to include the volume of some finest mesopores. The BJH-derived micropore volumes are significantly larger than those obtained by the *t*-plot method and change slightly from M-40 to M-56 (Table 2). Thus, the decrease of the BET surface area from M-40 to M-56 may be assigned mainly to the decrease of the fraction of small mesopores. For the monoliths M-68 and M-80, both *t*-plot-derived and BJH-derived micropore volumes decrease with respect to M-56, but the volume of mesopores increases. This leads to approximately equal specific surface areas of M-56, M-68, and M-80. Concluding, it should be noted that in order to obtain a more comprehensive picture of the microporous structure of the monoliths, more elaborate methods utilizing time-consuming nitrogen adsorption measurements at very low relative pressures are required.

3.4. Hydrodynamic characteristics and porosity

Hydrodynamic properties of a chromatographic column are very important since they determine the maximum flow rate at which the column can be operated. Fig. 5 shows the dependencies of the column pressure drop on the mobile phase flow rate for the obtained columns. All the dependencies are linear (R^2 = 0.9975–0.9999) in the studied ranges of flow rates and pressures, indicating that no compression of the monoliths occurs. Superficial-velocity-based permeability, k_p, was calculated for all the columns according to the Darcy equation [3]. Table 3 shows that permeability of the columns decreases by three orders of magnitude when the weight fraction of HEMA in the polymerization mixture increases from 4% to 8% (molar fraction of HEMA with respect to the total amount of monomers increases from 10.5% to 21.1%). To compare the monolithic columns with packed ones, permeability-equivalent particle diameter $d_{p,eqv}$, i.e., the particle diameter of a packed bed that would have the same permeability as the corresponding monolith, was calculated:

$$d_{p,eqv} = \sqrt{\varphi k_p} \quad (4)$$

where φ is the flow resistance parameter which is close to 1000 for a typical packed column with external (interparticle) porosity of about 0.4. Thus, the monolith M-40 has the permeability similar to that of a column packed with spherical particles with diameter of 32 μm while the permeability of M-80 is extremely low and comparable to that of a column packed with 1.1 μm particles.

Table 3
Hydrodynamic and porous characteristics of the obtained 150 mm × 3 mm i.d. poly(DVB-*co*-EVB-*co*-HEMA) monolithic columns.

Monolith	k_p (× 10^{12} m^2)[a]	$d_{p,eqv}$ (μm)[b]	d_{pore} (μm)[c]	ε_t (%)[d]		
				Pycnometry	Thiourea	Uracil
M-40	1.1	32.4	10.6	74.2	62.8	62.5
M-45	0.36	18.8	6.2	75.6	63.8	64.0
M-50	0.059	7.7	2.5	74.5	66.6	66.7
M-56	0.018	4.2	1.4	75.0	67.8	68.5
M-68	0.0028	1.7	0.55	75.0	n/a[e]	n/a[e]
M-80	0.0012	1.1	0.36	76.2	n/a[e]	n/a[e]

For the monolith designations, see Table 1.
[a] Superficial-velocity-based permeability. Mobile phase: acetonitrile.
[b] Permeability-equivalent particle diameter calculated according to Eq. (4).
[c] Average throughpore diameter estimated from the column permeability on the basis of the Kozeny model (Eq. (5)).
[d] Total porosity determined via pycnometry with acetonitrile and from the retention volume of uracil or thiourea with water/acetonitrile (50:50, v/v) as the mobile phase at 25 °C.
[e] Not available because of the low column permeability.

The average throughpore diameters of the monoliths were estimated from the permeabilities using the Kozeny model [32]. Considering porous monolith as a bundle of non-intersecting cylindrical capillaries with diameters equal to the monolith average throughpore diameter, one can obtain the following equation:

$$k_p = \frac{d_{\text{pore}}^2 \varepsilon_e}{32} \left(\frac{L}{L_{\text{pore}}} \right)^2 = \frac{d_{\text{pore}}^2 \varepsilon_e}{32} \sin^2 \alpha \quad (5)$$

where d_{pore} is the average throughpore diameter, ε_e is the external porosity of the column, L is the column length, L_{pore} is the average length of the throughpores, and α is the average angle between the throughpore and the column cross-section plane. Assuming $\varepsilon_e = 0.6$ and $\alpha = 45^\circ$, the throughpore diameters were calculated according to Eq. (5). The diameters obtained (Table 3) are in agreement with the pore sizes that can be estimated from the SEM images of the monoliths (Fig. 2).

The total porosities of the monoliths were determined via pycnometry and from the retention volumes of practically unretained compounds. In the latter case, uracil and thiourea were used as the hold-up volume markers. Table 3 indicates that all the columns have similar total porosities measured by pycnometry. The total porosity of a monolith is determined mainly by the volume of the porogen used for the column preparation and the volume of unreacted monomers. These volumes do not differ significantly for the monoliths considered. The extent of contraction of the liquid monomer mixture, which accompanies the polymerization process and contributes to the pore volume, also seems to be similar for all the prepared monoliths. The total porosities obtained with uracil as the hold-up volume marker are close to those obtained with thiourea, but significantly smaller than the values obtained via pycnometry. The difference can be accounted for by the larger extent of swelling of the polymers in pure acetonitrile compared to that in water-containing eluent, which results in opening of some micro- and mesopores blocked when water/acetonitrile mixture is used for the determination of the hold-up volumes. In part, the difference may also arise from the size exclusion of the molecules of uracil and thiourea from the finest permanent and gel-type [35] micropores accessible to the smaller molecules of acetonitrile. Table 3 also shows that porosities determined with uracil and thiourea grow from M-40 to M-56. This may be caused by the slight retention of these polar molecules, which increases with increasing polarity of the polymer. The weak retention of uracil and thiourea on the most hydrophilic column M-56 was confirmed by varying the column temperature. When the temperature decreases from 60 °C to 10 °C, the retention volumes of uracil and thiourea increase by 3.4% and 4.5%, respectively. However, the increase of the measured hold-up volume from M-40 to M-56 may be just a result of the improved swelling of more hydrophilic and less cross-linked polymers in the eluent or the decrease of the volume fraction of micropores which are inaccessible to uracil and thiourea, but accessible to acetonitrile. Eventually, the hold-up volumes obtained with water/acetonitrile solvent and uracil, which has molecular size close to the sizes of aromatic compounds employed for the chromatographic evaluation of the monoliths, were used for further calculations of chromatographic linear velocity and retention factors.

3.5. Column mechanical stability in water/acetonitrile mobile phases

Fig. 6 shows the pressure profile obtained when the monolith M-56 was gradually washed from pure acetonitrile eluent to pure water and back to acetonitrile. First, as the volume fraction of water in the mobile phase is increased, the backpressure increases in accordance with the growth of the mobile phase viscosity. When the percentage of water approaches 100%, the pressure

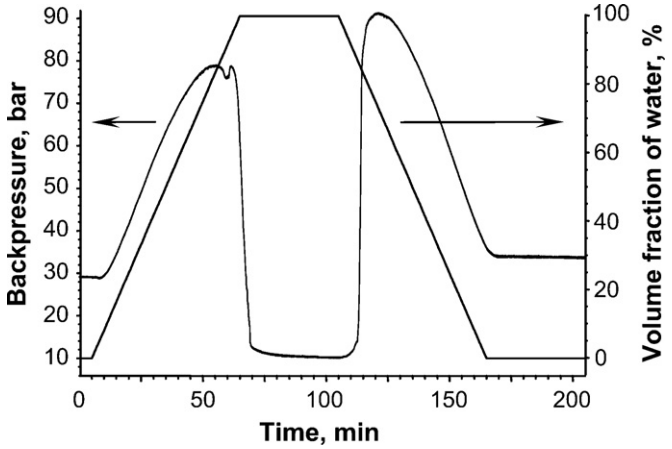

Fig. 6. Effect of the mobile phase composition on the mechanical stability of the obtained 150 mm × 3 mm i.d. poly(DVB-*co*-EVB-*co*-HEMA) monolithic column M-56. Mobile phase: water/acetonitrile, gradient from 100% acetonitrile to 100% water and back to 100% acetonitrile. Column temperature: 30 °C.

falls abruptly to the level lower than that of pure acetonitrile. This fall is explained by the shrinkage of the polymer in highly aqueous mobile phase, which results in detachment of the monolith from the column wall and the onset of the mobile phase flow in between the rod and the wall. As the mobile phase gradient is reversed to the lower fraction of water, the polymer swells again and seals the void between the rod and the wall; this leads to the steep rise of the pressure. Since the covalent bonding of the polymer to the wall has been broken, swelling of the monolith and the rise of pressure result in compression of the monolithic rod and irreversible loss of the efficiency of the chromatographic column. Finally, the pressure lowers according to the decrease of the mobile phase viscosity.

Pictures similar to that shown in Fig. 6 were observed for the other obtained poly(DVB-*co*-EVB-*co*-HEMA) monoliths. Thus, in the studied range of the monomer mixture compositions, the amount of HEMA in the polymer has little influence on the column mechanical stability in water-rich mobile phases. Higher amount of HEMA would probably result in more stable columns. However, the maximum fraction of HEMA in the polymerization mixture that in the studied polymerization conditions allows obtaining the column with high enough permeability is only 5.6 wt% (14.7 mol% with respect to the total amount of monomers). To increase the polarity of the monolith and its wettability with water further, other polymerization conditions (porogen, hydrophilic monomer) are required. It should be noted, however, that the use of highly aqueous mobile phases with the columns obtained is unnecessary since it results in too strong retention of the aromatic compounds used for evaluating the chromatographic performance. It was found that the monolith M-56 withstands flushing with 1000 column hold-up volumes of water/acetonitrile (60:40, v/v) mixture at as high column pressure drop as 100 bar without appreciable loss of efficiency.

3.6. Chromatographic properties

The main purpose of this work was to prepare monolithic rod columns based on poly(DVB-*co*-EVB-*co*-HEMA) and study the effect of the fraction of HEMA in the monomer mixture on the reversed-phase separation of small molecules with these columns. Fig. 7 shows the chromatograms of the mixture of aromatic compounds obtained with water/acetonitrile (40:60, v/v) as the mobile phase on the four prepared columns that exhibited reasonably high permeability. The main characteristics of the separation are outlined in Table 4. It is evident that the columns exhibit high selectivity,

Table 4
Parameters of the separation of a mixture of aromatic compounds on the obtained 150 mm × 3 mm i.d. poly(DVB-*co*-EVB-*co*-HEMA) monolithic columns[a].

Parameter	Monolith	Compound						
		Uracil	Pyridine	Nitrobenzene	Benzene	Toluene	Ethylbenzene	Propylbenzene
Retention factor	M-40	0	0.43	2.6	3.1	4.5	6.4	9.3
	M-45	0	0.40	2.3	2.8	4.1	5.8	8.4
	M-50	0	0.34	1.9	2.3	3.4	4.8	7.0
	M-56	0	0.32	1.7	2.1	3.1	4.3	6.2
Peak tailing factor[b]	M-40	1.18	1.30	n/a[c]	n/a[c]	1.24	1.23	1.24
	M-45	0.95	1.15	n/a[c]	n/a[c]	1.18	1.18	1.20
	M-50	1.23	1.35	n/a[c]	n/a[c]	1.38	1.39	1.41
	M-56	0.96	0.98	n/a[c]	n/a[c]	1.24	1.28	1.34
HETP (μm)	M-40	188	199	n/a[c]	n/a[c]	241	253	261
	M-45	171	166	n/a[c]	n/a[c]	188	198	204
	M-50	111	106	119	122	132	140	148
	M-56	51	53	60	62	70	76	83

For the monolith designations, see Table 1.
[a] Mobile phase: water/acetonitrile (40:60, v/v). Flow rate: 0.5 ml/min (u = 1.4–1.5 mm/s). Column temperature: 25 °C. Injection volume: 1 μl.
[b] Tailing factor, T, was calculated according to the following equation: $T=(a+b)/2a$, where a is the width from the front of the peak to the center of the peak at 5% height, b is the width from the center of the peak to the tail of the peak at 5% height.
[c] Not available because of insufficient resolution of peaks.

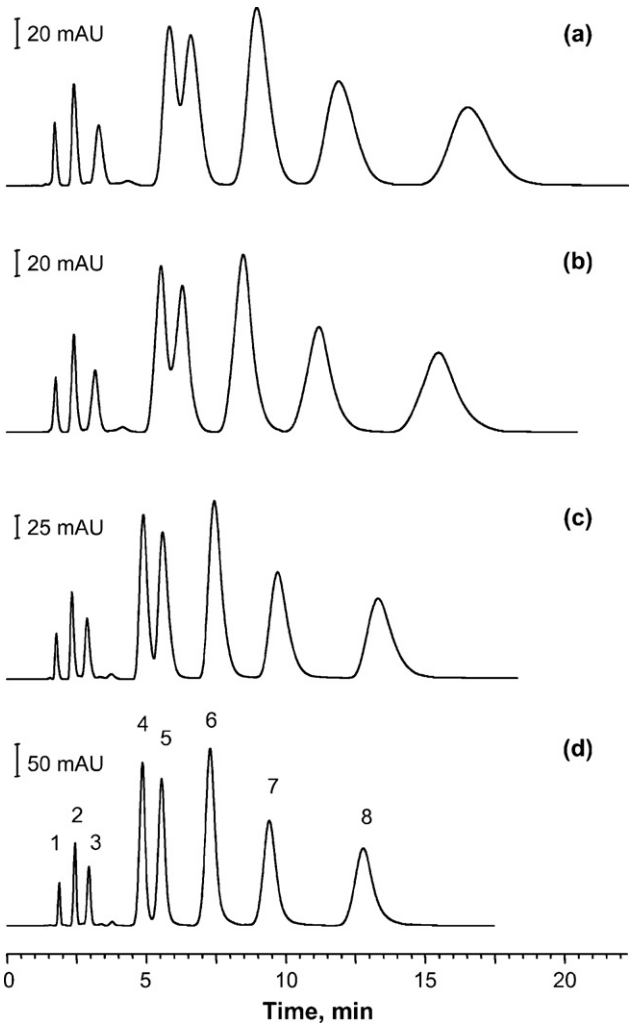

Fig. 7. Chromatograms of a mixture of aromatic compounds on the obtained 150 mm × 3 mm i.d. poly(DVB-*co*-EVB-*co*-HEMA) monolithic columns: (a) M-40, (b) M-45, (c) M-50, and (d) M-56. Mobile phase: water/acetonitrile (40:60, v/v). Flow rate: 0.5 ml/min (u = 1.4–1.5 mm/s). Column temperature: 25 °C. Injection volume: 1 μl. Peaks: (1) uracil, (2) pyridine, (3) impurity, (4) nitrobenzene, (5) benzene, (6) toluene, (7) ethylbenzene, and (8) propylbenzene. For the monolith designations, see Table 1.

and the chromatographic peaks have rather symmetrical shapes. When the amount of HEMA in the monolith increases, the column efficiency grows markedly, with the HETP being as low as 51 μm for M-56, and the separation time lowers.

All the HETP data were corrected for the extra-column contribution using Eq. (2). Unexpectedly, the corrected HETPs for most analytes on all the columns are higher than the uncorrected ones. In general, the difference increases with the decrease of the retention factor of the analyte. For unretained uracil on the least efficient column M-40, the difference approaches 10%. Seemingly, in this case the extra-column volume contributes more to the gross retention time of the analyte than to the band broadening, thus increasing the apparent column efficiency in comparison with the actual efficiency calculated with Eq. (2). Also such a result might be accounted for by the underestimation of the extra-column contribution to the peak variance when the peak-width at half height is used as the measure of band dispersion. However, calculation of the HETPs using the method of statistical moments [3,36] gives similar result: the corrected HETPs for most analytes are higher than the uncorrected ones. Unfortunately, the method of moments is very sensitive to the choice of the limits for peak integration, leading to relatively low precision of the HETP data; consequently, we report only the data based on the peak-widths at half height. The corrected HETPs for uracil obtained at different eluent velocities on the most efficient column M-56 are up to 15% lower than the uncorrected ones. In this case, the contribution of band broadening in the extra-column volume becomes more significant than it is for the less efficient columns.

For all the monoliths, the influence of the mobile phase composition on retention of toluene was investigated. The mobile phases studied were solutions of 40%, 50%, 60%, and 80% (v/v) of acetonitrile in water, and pure acetonitrile. The logarithm of the retention factor of toluene, $\lg k'$, was found to decrease with the increase of the volume fraction of acetonitrile, x, in the mobile phase. The obtained dependencies can be adequately approximated ($R^2 > 0.9983$) with the following equation [37]:

$$\lg k' = a - bx + cx^2 \quad (6)$$

where a, b, and c are positive parameters. This confirms typical reversed-phase mechanism of retention on the obtained monoliths.

Fig. 8 shows the plot of the logarithm of the retention factor of alkylbenzenes versus the number of alkyl carbon atoms. All the dependencies in Fig. 8 are linear ($R^2 > 0.9992$), and their slopes change only slightly (from 0.160 for M-40 to 0.156 for M-

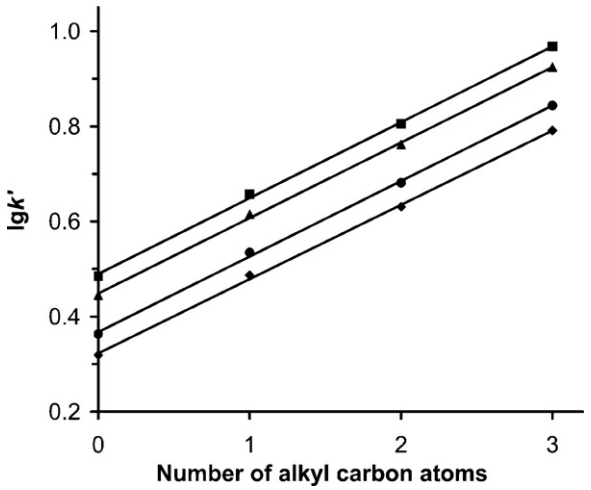

Fig. 8. Plot of the logarithm of the retention factor of alkylbenzenes versus the number of alkyl carbon atoms for the obtained 150 mm × 3 mm i.d. poly(DVB-*co*-EVB-*co*-HEMA) monolithic columns: (■) M-40, (▲) M-45, (●) M-50, and (♦) M-56. Mobile phase: water/acetonitrile (40:60, v/v). Column temperature: 25 °C. For the monolith designations, see Table 1.

56), indicating similar methylene selectivity of all the columns, while the absolute values of retention factors decrease. The latter is, obviously, a result of the improvement of polarity of the stationary phase. The reduction of retention, together with the improved efficiency and high selectivity, affords significant reduction of the separation time and consumption of acetonitrile with the column M-56 compared to the other obtained columns.

To investigate the kinetic performance of the fabricated columns, the effect of the eluent velocity on the HETP was studied for unretained uracil and for toluene under conditions of strong retention, with water/acetonitrile (50:50, v/v) as the mobile phase. The maximum flow rate applied was 3 ml/min, resulting in chromatographic velocity of about 9 mm/s, for M-40 and M-45. The maximum velocity for M-50 and M-56 was limited by the maximum backpressure of 100 bar to avoid compression of the polymeric rods. The obtained plot of the HETP against the chromatographic velocity is presented in Fig. 9. The solid lines in Fig. 9

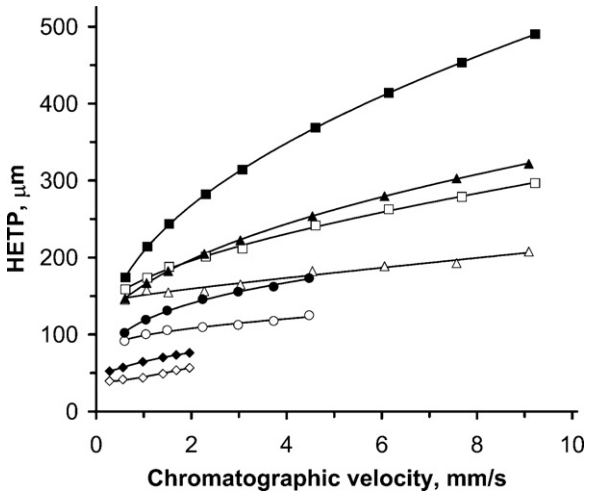

Fig. 9. Plot of the HETP versus the mobile phase chromatographic velocity for toluene (closed symbols) and uracil (open symbols) on the obtained 150 mm × 3 mm i.d. poly(DVB-*co*-EVB-*co*-HEMA) monolithic columns: M-40 (squares), M-45 (triangles), M-50 (circles), and M-56 (diamonds). Solid lines represent the best fit to Eq. (3). Mobile phase: water/acetonitrile (50:50, v/v). Column temperature: 25 °C. Injection volume: 1 μl. Retention factors of toluene are 8.8, 8.0, 6.7, and 6.0 on M-40, M-45, M-50, and M-56, respectively. For the monolith designations, see Table 1.

represent the best fit of the HETP curves to Eq. (3). This equation is empirical and its parameters have no simple theoretical justification, but it is simple and frequently used to approximate experimental data. Parameters of the best fit obtained are given in Table 5. Although the retention factors of toluene on the four columns are different, Fig. 9 and Table 5 allow making several conclusions since the column efficiency for the strongly retained compounds changes only slightly with the increase of retention (see Table 4).

The curves in Fig. 9 exhibit convex upward shapes, except for the curve of uracil on M-56. This observation is confirmed by the non-zero values of parameters A and n shown in Table 5. The zero values of coefficient B are just a mathematical consequence of the fitting procedure since the left branch of the HETP curve controlled by molecular diffusion was not observed at the lowest studied velocities for all the monoliths. Theoretically sound expression describing the band broadening in a chromatographic column can be written as [38]:

$$H = \sum_i \left(\frac{1}{A_i'} + \frac{1}{D_i' u} \right)^{-1} + \frac{B'}{u} + C_m u + C_s u \quad (7)$$

where the first term on the right-hand side represents the sum of different eddy diffusion processes contributing to the HETP in accordance with Giddings' coupling theory [39], the second term reflects the contribution of axial molecular diffusion, and the third and fourth terms represent the mobile and the stationary zone mass transfer resistance contributions, respectively. Although the interstitial rather than the chromatographic velocity should be used in Eq. (7), the former is proportional to the latter, with proportionality coefficient being the ratio of the column total porosity to the external porosity. Therefore, Eq. (7) can be applied to estimating the impact of different band broadening phenomena on the HETP. Depending on the model used, C_m-term can be a function of velocity, resulting in the proportionality of $C_m u$-term to velocity in the power smaller than unity [38]. Considering this fact, one may treat the first term of Eq. (3) as an analog of the sum of the eddy diffusion and the mobile zone mass transfer resistance terms of Eq. (7), the latter two terms being the only contributions that can account for the convexity of the obtained HETP curves. The mobile zone mass transfer resistance usually grows with the increase of retention factor [38] while the eddy diffusion contribution to the HETP, as has been recently shown [40], decreases with increasing retention. Since the convexity of the curves in Fig. 9 is more pronounced for retained toluene than for unretained uracil, this convexity to a large extent arises from the mobile zone mass transfer resistance. The slopes of the HETP curves are higher for toluene than for uracil and decrease from column M-40 to M-56. The high slope of the curve of toluene on M-40 indicates the high overall mass transfer resistance, which at high mobile phase velocities leads to a large difference in the column efficiency for retained and unretained compounds. At lower velocities, the role of the slow mass transfer vanishes, and this difference in efficiency becomes smaller. The highest overall mass transfer resistance in M-40 results from the largest domain size of this monolith evidenced by the SEM images (Fig. 2) and permeability measurements. With the growth of the domain size, both C_m- and C_s-term of Eq. (7) increase. Also the significant fraction of very small mesopores in M-40 (Fig. 4) and pore network effects indicated by the type H2 hysteresis loop of the nitrogen adsorption–desorption isotherm (Fig. 3) can hinder the diffusion in the stationary zone and increase the C_s-term of Eq. (7). When the amount of HEMA in the monolith increases, the domain size, as well as the volume of the finest mesopores, falls. This results in the lowest mass transfer resistance in M-56 among the four columns.

Table 5
Parameters of the best fit of the obtained dependencies of HETP on chromatographic velocity to Eq. (3).

Monolith	Parameter									
	A (μm (s/mm)^n)		n		B (μm mm/s)		C (μm s/mm)		R^2	
	U[a]	T[b]	U[a]	T[b]	U[a]	T[b]	U[a]	T[b]	U[a]	T[b]
M-40	160	201	0.163	0.335	4.3	0	7.3	7.4	0.9982	0.9999
M-45	145	153	0.022	0.278	0	7.0	5.9	4.4	0.9662	0.9999
M-50	96	118	0.096	0.254	0	0	2.7	0	0.9756	0.9972
M-56	30	62	0	0.275	1.6	2.3	12.9	0	0.9878	0.9997

For the monolith designations, see Table 1. For the analyses conditions, see Fig. 9.
[a] Uracil.
[b] Toluene.

In recent papers [9,10], Nischang et al. explained the poor performance of polymeric monoliths in the separation of strongly retained small molecules by the high resistance to mass transfer in the stationary zone caused by the presence of the gel porosity in the structure of swollen polymers. For the monoliths considered in this work, the gel porosity increases from M-40 to M-56 since the amount of cross-linker decreases in the same order, but the mass transfer resistance lowers. Thus, in comparison with the drop in the monolith domain size, the increase of the gel porosity has minor impact on the overall mass transfer resistance in the obtained monoliths.

Eddy diffusion is another important factor affecting the column efficiency. The minimum values of HETP measured for uracil on the prepared columns decrease from 159 μm for M-40 to 40 μm for M-56. Assuming that at the lowest studied velocities the mass transfer resistance contribution to the HETP of uracil becomes negligible while the eddy diffusion term reaches the velocity-range in which it grows slowly, one can attribute this drop in the HETP to the decrease of the eddy diffusion from M-40 to M-56, which can be explained by the reduction of the domain size of the monoliths.

For the monolith M-80 had extremely low permeability, its chromatographic properties were not studied. The efficiency of M-68 was evaluated by running analyses of the solution of toluene at flow rates of 0.1 ml/min and 0.2 ml/min (corresponding linear velocities about 0.25 and 0.5 mm/s) with pure acetonitrile as the mobile phase. The chromatographic peaks of toluene were symmetric (tailing factors < 1.03), and the HETP changed only slightly (from 53 μm to 51 μm) when velocity increased. The obtained HETP values are somewhat higher than expected taking into account very small domain size of M-68. This may be caused by the wide pore size distribution (Fig. 4), increased gel porosity, or probably higher bed heterogeneity of M-68 in comparison with the other obtained monoliths.

4. Conclusions

In this study, a series of poly(divinylbenzene-*co*-ethylvinylbenzene-*co*-2-hydroxyethyl methacrylate) monolithic rod columns with different monomer ratios were obtained and applied to the reversed-phase separation of low-molecular-weight aromatic compounds. The increase of the molar fraction of HEMA in the starting monomer mixture from 10.5% to 21.1% was found to have little influence on the column mechanical stability in water-rich mobile phases, with the most efficient column being stable in water/acetonitrile eluents containing up to 60% of water under pressures up to 100 bar. It was shown that higher HEMA amount in the polymerization mixture with 1-dodecanol as the porogen reduced the domain size of the monoliths, resulting in lower hydrodynamic permeability and improved column efficiency in the separation of small molecules.

Acknowledgements

This work was supported by Russian Foundation for Basic Research (grant no. 10-03-00215-a). The authors kindly thank Alexey V. Garshev (MSU) for conducting SEM. Andrey V. Smirnov, Ludmila I. Rodionova, and Elena E. Knyazeva (MSU) are thanked for the nitrogen adsorption measurements and valuable discussion.

References

[1] F. Svec, T.B. Tennikova, Z. Deyl (Eds.), Monolithic Materials: Preparation, Properties, and Applications, Elsevier, Amsterdam, 2003.
[2] N. Tanaka, H. Kobayashi, N. Ishizuka, H. Minakuchi, K. Nakanishi, K. Hosoya, T. Ikegami, J. Chromatogr. A 965 (2002) 35.
[3] G. Guiochon, J. Chromatogr. A 1168 (2007) 101.
[4] M.R. Buchmeiser, Polymer 48 (2007) 2198.
[5] N.W. Smith, Z. Jiang, J. Chromatogr. A 1184 (2008) 416.
[6] F. Svec, J. Sep. Sci. 27 (2004) 1419.
[7] E.G. Vlakh, T.B. Tennikova, J. Chromatogr. A 1216 (2009) 2637.
[8] F. Svec, J. Chromatogr. A 1217 (2010) 902.
[9] I. Nischang, O. Brüggemann, J. Chromatogr. A 1217 (2010) 5389.
[10] I. Nischang, I. Teasdale, O. Brüggemann, J. Chromatogr. A 1217 (2010) 7514.
[11] Z. Xu, L. Yang, Q. Wang, J. Chromatogr. A 1216 (2009) 3098.
[12] A. Greiderer, L. Trojer, C.W. Huck, G.K. Bonn, J. Chromatogr. A 1216 (2009) 7747.
[13] S.H. Lubbad, M.R. Buchmeiser, J. Chromatogr. A 1217 (2010) 3223.
[14] J. Urban, F. Svec, J.M.J. Fréchet, J. Chromatogr. A 1217 (2010) 8212.
[15] L. Trojer, S.H. Lubbad, C.P. Bisjak, W. Wieder, G.K. Bonn, J. Chromatogr. A 1146 (2007) 216.
[16] B. Mayr, G. Hölzl, K. Eder, M.R. Buchmeiser, C.G. Huber, Anal. Chem. 74 (2002) 6080.
[17] F. Svec, J.M.J. Fréchet, Chem. Mater. 7 (1995) 707.
[18] R.W. Allington, S. Xie, T. Jiang, M. Xu, Separation system, components of a separation system and methods of making and using them, US patent application 2008/0179773 A1 (2008).
[19] S. Hjertén, J.-L. Liao, R. Zhang, J. Chromatogr. 473 (1989) 273.
[20] A.M. Nguen, N.P. Dinh, Q.M. Cam, T. Sparrman, K. Irgum, J. Sep. Sci. 32 (2009) 2608.
[21] S. Xie, Monolithic column, US patent application 2009/0184039 A1 (2009).
[22] S. Xie, F. Svec, J.M.J. Fréchet, Chem. Mater. 10 (1998) 4072.
[23] J. Vidič, A. Podgornik, A. Štrancar, J. Chromatogr. A 1065 (2005) 51.
[24] F. Gritti, G. Guiochon, J. Chromatogr. A 1169 (2007) 125.
[25] J.H. Knox, J. Chromatogr. A 960 (2002) 7.
[26] S. Brunauer, P.H. Emmett, E. Teller, J. Am. Chem. Soc. 60 (1938) 309.
[27] E.P. Barrett, L.G. Joyner, P.P. Halenda, J. Am. Chem. Soc. 73 (1951) 373.
[28] W.D. Harkins, G. Jura, J. Chem. Phys. 11 (1943) 431.
[29] G. Glöckner, Polymer Characterization by Liquid Chromatography, Elsevier, Amsterdam, 1986.
[30] C. Viklund, F. Svec, J.M.J. Fréchet, Chem. Mater. 8 (1996) 744.
[31] K.S.W. Sing, D.H. Everett, R.A.W. Haul, L. Moscou, R.A. Pierotti, J. Rouquerol, T. Siemieniewska, Pure Appl. Chem. 57 (1985) 603.
[32] S. Lowell, J.E. Shields, M.A. Thomas, M. Thommes, Characterization of Porous Solids and Powders: Surface Area Pore Size and Density, Kluwer Academic Publishers, The Netherlands, 2004.
[33] K.K. Unger, R. Skudas, M.M. Schulte, J. Chromatogr. A 1184 (2008) 393.
[34] B.P. Santora, M.R. Gagn, K.G. Moloy, N.S. Radu, Macromolecules 34 (2001) 658.
[35] K. Jerabek, Anal. Chem. 57 (1985) 1598.
[36] F. Gritti, A. Felinger, G. Guiochon, J. Chromatogr. A 1136 (2006) 57.
[37] P. Jandera, H. Colin, G. Guiochon, Anal. Chem. 54 (1982) 435.
[38] G. Desmet, K. Broeckhoven, Anal. Chem. 80 (2008) 8076.
[39] J.C. Giddings, Dynamics of Chromatography, Marcel Dekker, New York, 1965.
[40] F. Gritti, G. Guiochon, J. Chromatogr. A 1217 (2010) 6350.